AD-A154 248   PRECIPITATION ESTIMATION USING COLLOCATED GOES   1/1
              SATELLITE AND SURFACE DATA(U) NAVAL POSTGRADUATE SCHOOL
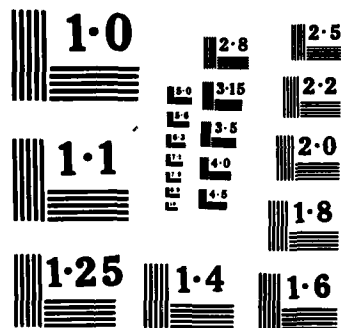   MONTEREY CA   D W RUST   DEC 84
UNCLASSIFIED   F/G 4/1   NL

END
FILMED

DTIC

NAVAL POSTGRADUATE SCHOOL
Monterey, California

THESIS

PRECIPITATION ESTIMATION USING COLLOCATED
GOES SATELLITE AND SURFACE DATA

by

David W. Rust

December 1984

Thesis Advisor: C. H. Wash

Approved for public release; distribution unlimited.

85   5   28   084

SECURITY CLASSIFICATION OF THIS PAGE (When Data Entered)

REPORT DOCUMENTATION PAGE	READ INSTRUCTIONS BEFORE COMPLETING FORM

1. REPORT NUMBER	2. GOVT ACCESSION NO. *A154 298*	3. RECIPIENT'S CATALOG NUMBER

4. TITLE (and Subtitle)	5. TYPE OF REPORT & PERIOD COVERED
Precipitation Estimation Using Collocated GOES Satellite and Surface Data	Master's Thesis December 1984
	6. PERFORMING ORG. REPORT NUMBER

7. AUTHOR(s)	8. CONTRACT OR GRANT NUMBER(s)
David W. Rust	

9. PERFORMING ORGANIZATION NAME AND ADDRESS	10. PROGRAM ELEMENT, PROJECT, TASK AREA & WORK UNIT NUMBERS
Naval Postgraduate School Monterey, California 93943	

11. CONTROLLING OFFICE NAME AND ADDRESS	12. REPORT DATE
Naval Postgraduate School Monterey, California 93943	December 1984
	13. NUMBER OF PAGES 69

14. MONITORING AGENCY NAME & ADDRESS(If different from Controlling Office)	15. SECURITY CLASS. (of this report)
	15a. DECLASSIFICATION/DOWNGRADING SCHEDULE

16. DISTRIBUTION STATEMENT (of this Report)

Approved for public release; distribution unlimited

17. DISTRIBUTION STATEMENT (of the abstract entered in Block 20, if different from Report)

18. SUPPLEMENTARY NOTES

19. KEY WORDS (Continue on reverse side if necessary and identify by block number)

Satellite Precipitation Specification
Satellite Meteorology
Bi-spectral Satellite Threshold
Objective Forecasting

20. ABSTRACT (Continue on reverse side if necessary and identify by block number)

The separation of precipitation from non-precipitation events using a matrix of GOES-E digitized infrared and visual satellite data was studied. Precipitation verification was conducted with collocated surface observations. The data set consists of 70,623 surface observations of which 29,342 have collocated satellite data.

The visual data were normalized and converted to albedos using the Muench and Keegan (1979) normalization scheme. The

DD FORM 1473 EDITION OF 1 NOV 65 IS OBSOLETE
1 JAN 73

S N 0102-LF-014-6601

1

data set was separated into four categories (precipitation/no-precipitation, and infrared/visual) and after testing for normality, it was determined that none of the categories were normally distributed. Using histograms, a distinct separation between the peaks of precipitating and non-precipitating events was found, but some overlap does exist.

Testing of infrared/visual thresholds for precipitation/no-precipitation events used in automated cloud and precipitation research yielded a correct estimation rate of 92% when the infrared and visual thresholds were combined.

Precipitation Estimation Using Collocated
GOES Satellite and Surface Data

by

David W. Rust
Captain, United States Air Force
B.A., University of St. Thomas, 1978

Submitted in partial fulfillment of the
requirements for the degree of

MASTER OF SCIENCE IN METEOROLOGY

from the

NAVAL POSTGRADUATE SCHOOL
December 1984

Author: _____
David W. Rust

Approved by: _____
C. H. Wash, Thesis Advisor

_____
J. S. Boyle, Second Reader

_____
Robert J. Renard, Chairman,
Department of Meteorology

_____
John N. Dyer,
Dean of Science and Engineering

ABSTRACT

The separation of precipitation from non-precipitation events using a matrix of GOES-E digitized infrared and visual satellite data was studied. Precipitation verification was conducted with collocated surface observations. The data set consists of 70,623 surface observations, of which 29,342 have collocated satellite data.

The visual data were normalized and converted to albedos using the Muench and Keegan (1979) normalization scheme. The data set was separated into four categories (precipitation/no-precipitation, and infrared/visual) and after testing for normality, it was determined that none of the categories were normally distributed. Using histograms, a distinct separation between the peaks of precipitating and non-precipitating events was found, but some overlap does exist.

Testing of infrared/visual thresholds for precipitaion/ no-precipitation events used in automated cloud and precipitation research yielded a correct estimation rate of 92% when the infrared and visual thresholds were combined.

TABLE OF CONTENTS

LIST OF TABLES

LIST OF FIGURES

I. INTRODUCTION

Every day, military and civilian forecasters are tasked to provide weather forecasts for remote areas of the world. Many are short-range forecasts (up to 12 h) for specific locations, rather than large areas. Facsimile charts combined with climatology provide reasonable wind and temperature forecasts, which can be cross-checked using satellite imagery. In addition, satellite imagery aids in preparing sky coverage forecasts. A major remaining problem is precipitation. Since there may be few, if any, timely surface observations available, it can be difficult to determine whether precipitation is falling beneath areas of cloud cover. What is required are methods to differentiate precipitation from non-precipitation using geostationary visual and infrared satellite data.

Research in this area is important for two interchangeable reasons. First, better observations will lead to better forecasts. A fundamental problem with all forecasting schemes is a lack of reliable initial data. An accurate and reliable scheme for differentiating between precipitating and non-precipitating clouds will greatly improve current and future forecasting schemes. Second, the use of satellite data will increase the area of coverage and therefore increase the number of potential observations. The more "good" initial data the better the chance the forecasting scheme will have to produce a better forecast.

Although microwave sensing has shown much promise in detecting rainfall, visible and infrared data are utilized in this research. A major drawback of microwave sensing is that it uses a broad field of view and has a more coarse resolution. In addition, visible and infrared data are currently more readily available (every 30 minutes).

Previously, studies have been undertaken which have attempted to correlate precipitation with satellite imagery. Muench and Keegan (1979) studied GOES-E visual and infrared satellite imagery and hourly rainfall climatological data for five surface stations in the northeastern United States for the period April through November 1977. Their data set consisted of 2760 surface observations, of which 300 reported precipitation. Using infrared and visual imagery, they attempted to predict hourly rainfall amounts. Although their results were "far from ideal", they were still "useful for making decisions if the threshold for 'action' versus 'no action' was known" (Muench and Keegan, 1979).

In addition to Muench and Keegan (1979), other researchers have studied this problem. Liljas (1981a, 1981b) developed a bi-spectral cloud classification based on visual and infrared data from the polar-orbiting TIROS-6 satellite. Lovejoy and Austin (1979), using the results of Muench and Keegan (1979), developed a two dimensional frequency plot for cumulus and non-cumulus precipitation. In addition, they also tested a spectral threshold technique for rain area mapping. For those unfamiliar with research in this area, a summary by Paul (1983) of selected studies included in Appendix A.

Paul (1983), using only daylight observations (0800L - 1600L EDT), computed means and standard deviations for each 10 x 10, 8 x 8, 6 x 6 and 4 x 4 matrix of pixels (both infrared and visual) centered on a surface reporting station with collocated geostationary satellite data. Her results showed a distinct separation between the means of the precipitation and non-precipitation cases. However, adding one standard deviation to the infrared precipitation mean and subtracting one standard deviation from the non-precipitation mean resulted in a significant overlap between precipitation and non-precipitation thresholds. This

11

percentage of moderate/heavy thunderstorms in the cold end than in the warm tail. These results showed only a slight increase (9% to 19%) in occurrence of heavier precipitation moving from the warm tail to the cold end. The major reason is that this study uses an average of surrounding points to generate a collocated satellite observation, whereas other studies, which show a distinct increase in precipitation intensity with colder cloud top temperatures, used the coldest cloud top temperature as the value.

In summary, although the occurrences of moderate/heavy precipitation were less than expected, the trend of increasing intensity with colder cloud top temperatures was present. Also, the trend of increasing thunderstorms and decreasing rain showers with colder cloud top temperatures is consistent with expectations.

5. Precipitation, Visible

This category consists of all observations which reported precipitation and had collocated visible satellite data (see Fig. 6). There were 1437 observations within this category. The distribution is as one would expect for a precipitation with visible satellite data category (albedo values clustered near the bright end). The estimated albedos ranged from 0.00 to 1.20. There is a peak of 132 observations between 0.65 and 0.70. The mean albedo is 0.61 with a standard deviation of 0.29.

This distribution was divided into three areas and further analyses were conducted on the dim tail (albedos less than 0.40), the bright tail (albedos greater than 0.90), and the region between the dim and the bright tails (see Table VI). The dim tail was chosen because it is the area of the greatest probability of misclassified observations. The other two areas were chosen to compare to the dim tail. Within each of the three areas, an analysis for

A possible reason why some precipitation precipitation observations have such warm cloud tops is because the precipitation, in addition to being light, is also very scattered. In this situation, a portion of the satellite data is composed of surface reports rather than cloud top data. Also, it should be noted that the surface observations are taken 5-10 minutes before the hour, while the satellite scan is taken 5 minutes after the hour. This 10 to 15 minute lag in the satellite scan is at least partially responsible for some of the misclassified observations. Precipitation could be reported at the surface station at the observation time, but by the satellite scan time, it may have stopped. This would produce a surface precipitation report with a collocated no-precipitation satellite report.

In the cold end there were 959 observations. Light thunderstorms were reported 42% of the time with light rain showers being reported 20% of the time. In addition, 15% of the observations reported moderate/heavy thunderstorms and 14% reported light rain. There were more light precipitation reports (81%) than moderate/heavy reports (19%). Once again convective type precipitation (79%) was reported more often than stratiform precipitation (21%).

In the region between the warm tail and the cold end there were 640 observations. Light rain showers were in 37% of the observations, followed by light rain in 29% and light thunderstorms in 21% of the observations. Light precipitation was reported in 89% of the observations, with moderate/ heavy precipitation in the remaining 11%. As before, convective type precipitation (66%) was reported more often than stratiform precipitation (34%).

It should be noted here that this study cannot distinguish between precipitation intensities with any degree of accuracy. One would expect a much higher

24

category. The distribution of cloud top temperatures (clustered near the cold end) is similar to what would be expected for a precipitation category. The cloud top temperatures ranged from a minimum of 205.0 K to a maximum of 296.6 K. It has a peak of 181 observations between 220.0 K and 225.0 K. The mean is 243.0 K with a standard deviation of 21.7 K.

Further analyses were conducted on the warm tail (warmer than 270.0 K), the cold end (colder than 240.0 K), and the area between them (see Table V). The warm tail was analyzed because it would most likely contain misclassified observations. The cold end and the middle area each were analyzed to better understand the satellite data distribution. Each of the three areas were analyzed for the type and intensity of the precipitation, and for convective versus stratiform precipitation.

In the warm tail there were 257 observations. Light rain showers were dominate with 50% of the observations. Light rain and light thunderstorms followed in frequency with 21% and 18%, respectively. An overwhelming majority, 91%, reported light precipitation, compared to only 9% with moderate/heavy precipitation. In addition, 76% of the observations were convective in nature compared to 24% of a stratiform nature. One can expect the observations within the warm tail to be misclassified because precipitation is not usually associated with warm cloud top temperatures. It should be noted though, that only 9% of the precipitation observations within the warm tail reported moderate or heavy precipitation, whereas 91% reported light precipitation. This leads one to conclude that although the observations within the warm tail could be misclassified, they would would be light precipitation and not moderate/heavy observations.

restriction on the data base. excluded most of the problems associated with distortion caused by low solar angles near sunrise and sunset. Because this study did not restrict the data base to a specific time period, distortion was a problem. In the distribution for this category there were 336 reports with albedos greater than 1.15. Further analysis of these reports showed all albedos greater than 1.15 were reported at 0000 GMT (near sunset). In addition, 83% of all observations with albedos greater than 0.70 occurred within three hours of sunrise or sunset. In addition to high albedo values caused by distortion or nearby precipitation, further analysis showed that one-third (44/135) of the observations between 0.70 and 1.15 which reported low overcast ceilings also reported fog. It must be noted that although these observations were clustered around sunrise, they were still assigned higher albedo values than one would normally expect for fog. A significant portion of these bright non-precipitation observations are related to problems in normalizing the satellite data for low sun angle situations. More work is required in using the cloud brightness normalization before more quantitative use of the data can be made.

In summary, most of the bright tail is composed of thick high clouds or overcast/broken clouds with clouds also at lower levels. As in the no-precipitation, infrared category, significant errors arise when these bright clouds are interpreted as precipitating clouds. In addition, distortion due to low solar angles also causes misclassified bright albedo values.

4. Precipitation, Infrared

This category consists of all observations reporting precipitation and with collocated infrared satellite data (see Fig. 5). There were 1856 observations within this

precipitation/no-precipitation decision. The cold tail is composed mostly of thick high clouds or overcast/broken clouds with additional clouds at lower levels. Significant errors arise if these cold cloud tops are interpreted as precipitating clouds.

3. No-Precipitation, Visual

This category consists of all observations without precipitation and with collocated visual satellite data (see Fig. 3). There were 14,740 observations within this category. As expected, the majority of the observations are grouped near the dim end. The estimated albedos ranged from 0.00 to 1.20. It has a peak of 1944 observations at 0.00. The mean albedo was 0.27 with a standard deviation of 0.26.

Further analyses were conducted on the 999 observations comprising the bright tail (greater than 0.70) which would lead to misclassification of precipitation from the visual data. It was found that 49% of the observations reported overcast ceilings and 51% reported broken ceilings (see Table IV). Within the overcast ceiling category, 18% were high clouds, 14% were mid-level clouds, and 17% were low clouds. Within the broken category, 41% were high clouds, 7% were mid-level clouds, and 3% were low clouds. Combining the overcast ceilings with the broken ceilings produced 59% of the observations with high clouds, 22% with mid-level clouds, and 20% with low clouds. As in section D.2, the breakdown of the overcast ceilings can be misleading. To approximate the actual percentage of high clouds, further analyses were conducted on the high cloud with broken ceiling category for multi-layered clouds. It was found that 83% of those observations contained multi-layered clouds.

The large number of albedos between 1.15 and 1.20 is cause for concern. Paul (1983), by imposing a time

21

Combining the overcast ceilings with the broken ceilings produced 76% of the observations with high clouds, 16% with mid-level clouds, and 8% with low clouds.

The breakdown of the overcast ceiling category can be misleading. When an observer reports an overcast ceiling, he cannot see what is above the base of the clouds. The misrepresentation arises because the tops of the clouds are not at the level reported by the observer. In addition, there may be additional layers above the overcast layer. The satellite data will therefore contain information about the highest (coldest) clouds it senses and that layer may possibly be one or two layers above the reported ceiling.

To approximate the percentage of overcast ceilings affected, the high cloud with broken ceilings category was further analyzed. It was found that 95% of the observations within that category were multi-layered clouds (with either scattered or broken conditions reported at low or mid-levels in addition to a broken ceiling reported at the high level).

The overwhelming number of warm cloud top temperatures is not surprising for a non-precipitation category. Of some concern though, are the few temperatures (66) which exceed 300.0 K (27.0 C). One explanation is that the infrared sensor is seeing the top of a marine layer along the Gulf coast. Another possibility is that the surface of the earth is influencing the mean value of the 4 x 4 matrix. This is possible because one surface observation is representing a 424 sq n mi area. Just because a ceiling is being reported at the observation location, does not necessarily mean there is a ceiling 10 n mi away. Warm surface temperatures could increase the mean value of the matrix significantly.

In summary, the large majority of warm temperatures for non-precipitation cloud tops is just as one would expect. The extremely warm temperatures do not affect the

20

D. DISTRIBUTION CHARACTERISTICS

1. Introduction

This section will present a discussion about each of the histograms plotted for infrared/visual and no-precipitation/precipitation. It is important to remember that only broken or overcast ceilings are included in the distributions. Also, due to round-off error, not all percentages calculated in this section add up to 100% exactly.

2. No-Precipitation, Infrared

This category consists of all surface observations without precipitation and with collocated infrared satellite data (see Fig. 2). There were 19,354 observations within this category. As expected, the majority of the observations are grouped near the warm end. The cloud top temperatures ranged from a minimum of 205.0 K to a maximum of 320.1 K. It has a peak of 4214 observations between 290.0 K and 295.0 K. The mean temperature was 275.7 K with a standard deviation of 19.4 K.

The most interesting part of this distribution is the cold tail (less than 240.0 K). These are observations which would be misclassified by a single cold threshold. It was found that of the 1461 observations within the cold tail, overcast and broken ceilings were divided evenly (see Table III). Within the overcast ceiling category, 35% were high clouds with 10% mid-level clouds and 5% low clouds. Within the broken ceiling category, 41% were high clouds with 7% mid-level clouds and 3% low clouds. If two or more levels reported broken ceilings, the highest ceiling was specified as the ceiling for this study. For example, if a station reported 3500 broken, 10,000 broken, and 22,000 broken, the ceiling would be reported as a high ceiling.

19

Histograms were plotted for each of the four data categories with observations which had collocated satellite data. Within each category, a 10 x 10, 8 x 8, 6 x 6 and 4 x 4 matrix was also plotted. Even though the 4 x 4 matrix had already been chosen as the size to be evaluated, the option to change sizes if warranted by the normality testing was left open.

The Chi-square test was chosen to test the distribution for normality. It involves comparing a sample distribution to a normal distribution. Each distribution was divided into 20 bins. Using the mean and standard deviation computed earlier for each category, 17 degrees of freedom were available. All of the no-precipitation categories could be seen not to be normally distributed by inspection of the histograms (see Fig. 2 and Fig. 3) and therefore were not formally tested. Since each precipitation category more closely resembled a normal distribution, they were tested with the Chi-square test. Each no-precipitation distribution tested (all four matrix sizes) proved not to be distributed normally. Fig. 4, although appearing to be normally distributed, only had a 5% chance of coming from a normal distribution, and it was the closest to normal of any category tested.

It must be understood that just because a distribution has a low confidence level for being normally distributed, it does not mean that it is not a normal distribution. Likewise, just because a distribution has a high confidence level of being normally distributed, does not mean that it is a normal distribution. Since the results showed a high probability of not being normally distributed, the research focus shifted to describing the non-normal and other interesting aspects of the distributions.

II). From these results it was concluded that the distribution of the data would not change significantly as the matrix sizes were changed. The matrix size could now be based on meteorological parameters.

Initially one could argue that the 2 x 2 matrix would be the most representative. It could most accurately represent the surface observation by not being influenced as much by the surrounding area as any of the larger sizes. The major disadvantage of the 2 x 2 matrix though, is actually its small size. Because the navigational error of McIDAS is one to two pixels, the possibility that the surface observation would actually be outside the satellite data matrix is present. Choosing the 4 x 4 matrix would greatly reduce the possibility of having the surface observation outside the satellite data matrix. The 6 x 6 matrix would guarantee (within McIDAS error) the surface observation being within the matrix, but now areal coverage must be considered. The 6 x 6 matrix has an areal coverage of 729 sq n mi at 30 N while the 4 x 4 matrix covers 484 sq n mi, approximately 66% of the 6 x 6 matrix. After weighing the possibility of a misplaced observation using the 4 x 4 matrix, with the increased coverage of the 6 x 6 matrix, the 4 x 4 matrix was chosen as the most representative matrix size.

C. NORMALITY

The determination of the normality of the distributions within the data set was an important stipulation of this research. Since the normality determined the way in which the distributions could be described (using confidence levels if normal, and just general descriptions if not normal), it was paramount that the distribution be tested correctly.

17

III. DATA ANALYSIS

A. INTRODUCTION

This chapter consists of analyses and discussions of the data set. It begins with a discussion on choosing the most representative and reliable matrix size and the distributions formed by those matrices. Next, the distributions are tested for normality. Using those results, the distribution characteristics are described and discussed. Next the results are compared to those obtained by Paul (1983). In the final section, the data set is used to verify the established precipitation/no-precipitation thresholds of an automated cloud and precipitation estimation scheme (Wash et al, 1984) with the U. S. Navy's Satellite Data Processing and Display System (SPADS).

B. MATRIX SIZE

The collocated satellite data consisted of a 10 x 10 matrix centered on the surface observation station. This provided the option of using any one of nine different matrix sizes, 10 x 10 through 2 x 2, in the research. Paul (1983) evaluated four sizes, 10 x 10, 8 x 8, 6 x 6 and 4 x 4 (2025 sq n mi, 1296 sq n mi, 729 sq n mi and 484 sq n mi respectively). Her results (using 7358 no-precipitation observations and 534 precipitation observations) showed no significant differences in the means and standard deviations of the four matrices. When Paul's time restrictions were removed, the results (using up to 19,354 no-precipitation observations and 1856 precipitation observations) also showed no significant differences between the same four matrices based on the means and standard deviations (Table

16

group. The precipitation data category consists of all observations with an "R" in the current weather group.

The cloud cover group is based on a three digit code. The first digit indicates the amount of low clouds, where 0 is defined as clear, 1 is scattered, 2 is broken, and 3 is overcast. The definitions for clear, scattered, broken, and overcast are as defined in the Federal Meteorological Handbook No. 1 (U. S. Department of Commerce, 1980). The second and third digits of the cloud group indicate the amount of middle and high clouds respectively.

In this study there were no restrictions to a specific time frame. Rather, all observation, regardless of time, which had satellite data available were used. The only restrictions imposed were:

1. Only broken or overcast skies were considered; and

2. Each pixel count must be greater than zero.

Only broken or overcast ceilings were chosen to be analyzed, based on the assumption that precipitation from scattered skies is rare and that precipitation from clear skies is an incorrect observation. Indeed, Paul (1983) reported that less than one percent of the precipitation observations within her time period also reported scattered skies. The restriction that each pixel count be greater than zero was imposed because any pixel less than zero in meaningless.

Paul (1983) limited her time period to daylight hours only (0800 - 1600L EDT) to avoid distortion of the visible data due to low solar elevation angles. By choosing not to limit the time period for this study, it was understood that distortion of visible data may occur.

albedo values cannot exceed 1.00, this scheme allows values to overshoot 1.00 up to a value of 1.20. Therefore, the visual satellite values are not true albedos, but are estimated albedos. The extended visual normalized data scale was used to permit comparison of the results of this research to the bi-spectral threshold specifications of Muench and Keegan (1979) and to Paul (1983). The Muench and Keegan normalization scheme specifies that any computed albedo greater than 1.20 be set equal to 1.20 to limit unreasonably large values. Similarly, the scheme specifies computed albedos less than 0.15 be interpreted as the ground or water surface reflectance and the value 0.00 be assigned. (See Appendix B for further specific information concerning the Muench and Keegan normalization scheme.) The infrared data were processed in digital counts and converted to cloud top temperatures prior to statistical calculations.

The surface reports within the data set contain information that regularly appears in all Service-A reports, plus additional location information and visual and infrared satellite data (see Table I). Of the information available, we were most concerned with the current weather, the cloud group, and the satellite data.

For this study, the data set was divided into four categories:

1. Observations with no precipitation and infrared satellite data (19,354 Obs);

2. Observations with no precipitation and visual satellite data (14,740 Obs);

3. Observations with precipitation and infrared satellite data (1856 Obs); and

4. Observations with precipitation and visual satellite data (1437 Obs).

The no-precipitation data category is comprised of all observations not showing any "R" in the current weather

II. DATA DESCRIPTION

The data set assembled for this study consists of collo-
cated GOES-E satellite data and Service-A hourly surface
observations for the southeastern United States during
August 1977. During August, this region is dominated by
subtropical airmasses with extensive convective activity.
The GOES-E data consists of 10 x 10 pixel matrices of
visible and infrared satellite data centered over each of
137 reporting stations (Fig. 1), all south of 40 N. The
satellite data are measured with the Visual Infrared Spin
Scanned Radiometer (VISSR) which have subsatellite point
spatial resolutions of 1 km for visual channels and 7 km for
infrared channels (U. S. Department of Commerce, 1983) The
GOES-E navigation was completed by Man-computer Interactive
Data Access System (McIDAS) at the University of Wisconsin
using the full resolution visual data, with an accuracy of
1-2 pixels (1-2 km). The full resolution visual data were
averaged to a 7 km resolution, to equal the infrared data
resolution. The visual and infrared digital counts ranged
from values of 0-63 and 0-255, respectively. The 10 x 10
GOES-E visual and infrared satellite data each cover an area
of 45 n mi x 45 n mi at 30 N (60 n mi x 60 n mi at 42 N).

What distinguishes this data set from those used in most
other studies is the number of observations. This data set
has a total of 70,623 Service-A hourly reports, of which
29,342 reports have collocated visual and/or infrared satel-
lite imagery. The visual data were normalized and converted
to albedos based on the algorithm of Muench and Keegan
(1979). Their scheme corrects for the varying zenith angles
as well as adjusting the visual satellite data for aniso-
tropic scattering as related to the zenith angle. While

13

overlap was too large to permit an unbiased forecast to be made. Similar results were found using visual satellite data.

This research will concentrate on relating satellite imagery to observed precipitation and non-precipitation events using the surface-satellite data set of Paul(1983). The objectives are:

1. Use a full 24 h data base, vice the 9 h data base by Paul (1983);

2. Form distributions of satellite data for several classes of observed weather events, test for normality and study the separation of the distributions.

3. Apply established visual and infrared thresholds to the data set and determine their reliability.

This thesis is organized into four chapters. Chapter II describes the data set. Chapter III presents an analysis and discussion of the data set. Selection of matrix sizes for analyses and choices for studying the characteristics of each distribution are explained. Results are then compared to Paul (1983). The final section verifies the precipitation/no-precipitation infrared and visible thresholds currently used in SPADS. Chapter IV states conclusions and suggests further study.

precipitation type, precipitation intensity and convection or stratiform precipitation was conducted.

In the dim tail there were 327 observations. Light rain showers (43%) were dominate with light thunderstorms (28%) and light rain (15%) following in frequency. Light precipitation was reported in 88% of the observations with moderate/heavy precipitation in 12% of the observations. In addition, convective type precipitation was reported 81% of the time with stratiform precipitation being reported 19% of the time. As expected, most of the misclassified observations were light precipitation reports.

In the bright tail there were 165 observations. Light thunderstorms were reported in 29% of the observations with light rain being reported in 21% of the observations. Also, 19% of the observations were light rain showers and 18% were moderate/heavy thunderstorms. Light precipitation was reported more often (72%) than moderate/heavy precipitation (28%). Convective type precipitation was also reported in 72% of the observations as opposed to stratiform precipitation being reported in 28% of the observations. As expected, most of the moderate/heavy precipitation and thunderstorm observations were in the bright end.

In the region between the dim tail and the bright tail, there were 947 observations. Light rain showers and light thunderstorms were dominate in this region with 30% and 29% of the reports respectively. Light rain was reported in 22% of the observations. Light precipitation was reported in 83% of the observations while moderate/heavy precipitation was reported in 17% of the observations. Within this category, convective type precipitation was reported 74% of the time while stratiform precipitation was reported 26% of the time.

An important consideration when evaluating the visual categories is the time of day. In this category, 57%

of the observations were within a three hour period from 2200 to 0000 GMT. This implies that most of the precipitation occurs late in the afternoon. Also, 87% of the 0.00 estimated albedo values (39) occurred at 0000 GMT. Of the remaining 0.00 values, two occurred at 1300 GMT and one each at 2000 GMT, 2100 GMT, and 2300 GMT. This suggests that distortion caused some of the very low estimated albedo values.

E. COMPARISON OF RESULTS TO PAUL (1983)

1. Introduction

This section will compare our results with the results by Paul (1983). Paul (1983) divided her data into seven precipitation categories:

1. convective;
2. continuous;
3. light;
4. moderate/heavy;
5. general;
6. overcast ceiling; and
7. overcast and broken ceiling;

and two no-precipitation categories:

1. no-precipitation, overcast ceiling; and
2. no-precipitation, broken and overcast ceiling.

Each of the above nine categories were further divided into those with infrared satellite data and visible satellite data.

As stated previously, this study used one precipitation category and one no-precipitation category, each divided into a visible and an infrared satellite group. In addition, only those surface observations which reported either broken or overcast ceilings were evaluated.

27

This chapter is divided into two sections. One will compare results of the precipitation category and the other will compare results of the no-precipitation category.

2. Precipitation

This section will compare these results to those from Paul (1983) for the precipitation with broken or overcast ceilings (see Table VII). The mean values will be discussed first, followed by the standard deviations.

a. Means

The mean infrared values of this study are approximately 8.0 C colder than those from Paul (1983) (see Table VII). The differences can be attributed to the fact that nightime data are included in this study. In this area of the country many thunderstorms occur from late evening through the early morning hours. By including these storms (with their cold cloud top temperatures) in this study, the mean cloud top temperatures must decrease.

Also, the means of the infrared data decreased slightly (became colder) in both studies as the matrix size decreased. This decrease can be attributed to the decrease in surrounding area when changing from a 10 x 10 matrix to a 4 x 4 matrix. The smaller matrix size allows the satellite to detect only the colder cloud tops associated with the precipitation and not the warmer clouds from the fringe areas.

There was very little difference in the visible mean values between the two studies (see Table VII). This is not surprising because the time restrictions imposed by Paul (1983) contained most of the visible satellite data within the data set. The trend of the mean visual values is the same for both studies (see Table VII). Both show a slight increase in albedo values when changing from a 10 x 10 matrix to a 4 x 4 matrix.

28

b. Standard Deviations

The infrared standard deviations are slightly
larger in this study than in Paul (1983) (see Table VII).
The trend of increasing standard deviations with decreasing
matrix size occurs in both studies. This can be related to
the warmer fringe areas of the clouds being deleted by the
smaller matrices.

The standard deviations of the albedo values are
larger in this study than in Paul (1983) (see Table VII).
By restricting the time frame, Paul (1983) eliminated many
possible distorted values that were included in the calcula-
tions for this study. Since the distorted values tend to
accumulate at the extremes (0.00 and 1.20), including them
in the calculations increases the standard deviations.

The trend of the albedo standard deviation
values is toward slightly larger values as the matrix sizes
decrease. The less fringe area covered by the 4 x 4 matrix
diminishes the chances of the dimmer fringe area values
being included in the calculations.

3. No-precipitation

a. Means

The mean infrared values in this study are
approximately 4.0 C colder than those from Paul (1983) (see
Table VIII). The mean values of both studies remain almost
constant as the matrix size is decreased.

The visual means showed very little difference
between the two studies (see Table VIII). As stated before,
this is not surprising since most of the visual readings are
within the time restrictions imposed by Paul (1983). In
both studies, the mean albedo values tend to remain constant
as the matrix size is decreased.

b. Standard Deviations

The infrared standard deviations are about 1.5 C larger than Paul (1983) (see Table VIII). As in the precipitation category the standard deviations increase slightly as the matrix sizes decrease.

The standard deviations of the visible values are approximately 0.06 larger than those in Paul (1983) (see Table VIII). This can be attributed to the addition of distorted mean values in this study which were excluded by the time restrictions imposed by Paul (1983). The distorted values give additional weighting to each end of the range, causing the standard deviations to increase. The trend of the slightly increasing visual standard deviations with decreasing matrix sizes is again repeated here.

F. SPADS THRESHOLD VERIFICATION

This section will verify the no-precipitation/precipitation threshold of a cloud and precipitation analysis model of the United States Navy's interactive Satellite Data Processing and Display System (SPADS) using the 24 h data base. The objective is to present a comprehensive analysis of the infrared, visible, and infrared and visible thresholds combined. No attempt will be made to derive better thresholds, but only to verify the existing thresholds. After a brief explanation of the automated cloud and precipitation analysis program, there is a discussion on how thresholds work in an ideal situation. Next is an explanation on how the verification was conducted, and then the results are presented.

This program was designed to produce in real time (15 to 30 minutes) analyses of important cloud and weather features. It uses the Geostationary Observational Environmental Satellite (GOES) visual and infrared images to

30

produce contoured digital displays of cloud types, cloud
amounts, cloud top heights, cloud top temperatures, and
precipitation intensity for an approximate 1024 x 1024 n mi
sector of a geostationary image.

The objective was to determine the success of the
precipitation/no-precipitation thresholds in separating
precipitation from no-precipitation for this data set.
Ideally a threshold value will produce a clear and distinct
separation between two events. If the two distributions
overlap (an area with equal probability of either event
occuring), the smaller the overlap the better. The
threshold with an overlap can still be useful as long as
there is not too high a percentage of each event located
within the overlap region. The more events located within
the overlap region increases the chance of a misclassified
event up to a point where there is no longer any skill asso-
ciated with this prediction technique.

The verification was conducted using the entire data set
over the full 24 hours. The visual and infrared thresholds
from the interactive cloud and precipitation analysis
program were verified using the four categories described in
chapter II. The thresholds values used in the verification
were:

1. Estimated albedos greater than or equal to 0.55; and
2. Cloud top temperatures less than or equal to 249.0 K;
for precipitation, and:

1. Estimated albedos less than 0.55; and
2. Cloud top temperatures greater than 249.0 K;
for no-precipitation.

Using only the infrared threshold, the no-precipitation
and precipitation histograms (see Fig. 2 and Fig. 5) were
scanned for values which exceeded/were less than or equal to
249.0 K. The results (see Table IX) showed that 64% of the

31

precipitation observations had cloud top temperatures greater than or equal to 249.0 K. Likewise, 87% of the no-precipitation observations had cloud top temperatures less than 249.0 K.

Using only the visual thresholds, the no-precipitation and precipitation histograms (see Fig. 3 and Fig. 6) were scanned for values which were greater than or equal to/less than 0.55. The results (see Table X) showed that 63% of the precipitation observations had albedo values greater than 0.55. Likewise, 87% of the no-precipitation observations had albedo values less than 0.55.

Next the above calculations were repeated, only this time the criterion for precipitation/no-precipitation was based on both the visual and infrared satellite data. If an observation did not contain both visual and infrared satellite data, it was not considered in our calculations. The results are shown in Table XI. They show that 82% of all precipitation observations in the data set had both albedo values greater than or equal to 0.55 and cloud top temperatures less than or equal to 249.0 K. Likewise, 93% of the no-precipitation observations had albedos less than 0.55 and cloud top temperatures greater than 249.0 K. Using the visual/infrared thresholds together increases the chance of correctly classifying a precipitation event from 63% for visible and 64% for infrared to 82%. In addition, using the visual/infrared thresholds together increases the chance of correctly classifying a non-precipitation event from 87% for both visual and infrared to 93%.

G. SUMMARY

This chapter consisted of analyses and discussions of our data set. It began with a discussion on choosing the most representative and reliable matrix size and the

distributions formed by those matrices. Next the distributions were tested for normality. Using those results, a discussion of the characteristics of the distributions were presented. From there, the results were compared to those obtained by Paul (1983). The final section was a verification of the established precipitation/no-precipitation thresholds using the data set.

IV. SUMMARY AND CONCLUSIONS

A. DATA DESCRIPTION SUMMARY

A data set consisting of 70,623 surface observations, of which 29,342 had collocated satellite data, was studied. The satellite data consists of a 10 x 10 matrix centered on the surface observation station. The visual satellite data were converted to albedo values using the Muench and Keegan (1979) normalization scheme. This scheme also corrects for anisotropic scattering effects. The data set was divided into four categories of precipitation/no-precipitation and visual/infrared satellite data. It was further divided by using only those observations which reported broken or overcast ceilings. In addition, the full 24 hours of available data was analyzed, compared to the 9 hours of daytime observations used by Paul (1983).

B. DATA ANALYSIS SUMMARY

This chapter consisted of analyses and discussions of the data set. It was determined that the 4 x 4 matrix had the best combination of accuracy of location, and accuracy in best describing the region based on a single observation. Next, a description of how the histograms were formed and tested for normality was given. Because one could not say with any acceptable degree of confidence that the distributions were normally distributed, it was decided to analyze the non-normal parts and to gain a better understanding into the composition of the data set. The trends when moving from the cold/bright end to the warm/dim ends were as expected, but one could not accurately separate light from moderate/heavy precipitation using the cloud top

34

temperatures or albedos. When the results were compared to

Paul (1983), there were many similarities, especially when decreasing the size of the matrices from 10 x 10 down to 4 x 4.

The last area studied was the verification of established precipitation/no-precipitation thresholds used by the cloud and precipitation analysis scheme in SPADS with the data set. It was found that using both the visual and infrared satellite data together to determine precipitation/ no-precipitation produced the best results.

C. CONCLUSIONS

The conclusions of this study are:

1. Based on the results of the Chi-square test, the data set and all its subsets used in this study are not normally distributed;

2. The histograms for the precipitation/no-precipitation and infrared/visual categories each were distributed as one would expect for precipitation and no-precipitation events respectively;

3. Although the peaks of the precipitation/no-precipitation and infrared/visual distributions were as expected, the precipitation and no-precipitation distributions display partial overlap;

4. Investigation of the overlap areas indicates that multiple and thick high cloud layers are responsible for erroneous estimates of precipitation within the no-precipitation distributions. Concerning the precipitation distributions, the scattered character of the summertime precipitation likely produced a significant number of misclassifications;

5. Albedo estimates for the brightness normalization scheme are not reliable in the low sun angle situations; and

35

6. Estimates of reliability for precipitation/no-precipitation thresholds were obtained from the data set. Using both the infrared and visual precipitation/no-precipitation thresholds combined greatly improves the precipitation estimation when using each threshold separately.

D. SUGGESTED FURTHER STUDY

The recommendations for further study are:

1. Further analyses of precipitation categories should be conducted by separating them into specific precipitation types (i.e. thunderstorms, rain showers, etc);

2. Do additional studies of precipitation/no-precipitation thresholds for cloud/precipitation estimation; and

3. Gather and study additional collocated data sets in other seasons and for other regions.

APPENDIX A
PREVIOUS RESEARCH BY PAUL (1983)

A. BI-SPECTRAL AND INFRARED THRESHOLD

Liljas (1981a, 1981b) developed a bi-spectral cloud classification based on visual and infrared data from the polar orbiting TIROS-6 satellite (see Fig. 7). The data set consisted of a limited number of daily observations, chosen for their synoptic characteristics, in May and August 1979 over a region encompassing Norway, Sweden, Finland, and the Baltic Sea with weather charts providing the ground truth. Based upon the precipitation threshold results of Muench and Keegan (1979), Liljas chose a cloud top temperature threshold of -12 C to -15 C to classify cumulonimbus and nimbostratus clouds. Starting with this cloud classification and the assumption that the highest and the densest clouds produce the maximum precipitation amount, Liljas suggested a qualitative precipitation scale based on the sum of the visual and infrared satellite digital counts (see Table XII). These sums represent the areas of the Liljas nimbostratus and cumulonimbus cloud types in his bi-spectral cloud classification (see Fig. 8).

Lovejoy and Austin (1979) studied rain mapping of cloud areas based on GOES visual and infrared satellite data over Montreal, Canada, and the tropical Atlantic (Global Atmospheric Research Program Atlantic Tropical Experiment, GATE, data) with radar providing the ground truth. The Montreal data set consisted of 17 observations over three days during June 1977. Working with 4 x 4 resolution satellite image, Lovejoy and Austin plotted two dimensional frequency grids for the radar-determined rain and no-rain

37

points on a 25 x 25 array (See Fig. 9 and Fig. 10). The visual data were normalized by selecting the "brightest" and "dimmest" values in each image and linearly interpolating the radiances between 0 and 1.

Lovejoy and Austin (1979) state, with reference to the cumulus rain data distribution of Fig. 9 that, "The distribution was to a good approximation a two-dimensional Guassian." They do not provide or describe the statistics to support this assertion. The no-rain cumulus cases (Fig. 10) were described as a bimodal distribution with one peak near the low visual and low infrared values and the other peak near the rain peak but shifted slightly toward lower values. In most cases, the separation of the cumulus rain and no-rain cases was statistically significant with the probability ranging from 10% to 50% that the rain and no-rain samples came from the same population.

The Lovejoy and Austin (1979) two dimensional frequency plots for non-cumulus storms were limited to one case. The significant differences between the cumulus and non-cumulus data sets were the non-cumulus no-rain plot lost its bimodal character, relative to the cumulus no-rain plot, and appeared as a broad two dimensional Gaussian distribution. The non-cumulus rain plot points fell within the no-rain distribution, but were shifted slightly higher in the visual. The separation of the non-cumulus rain and no-rain cases was not statistically significant, with greater than a 50% probability of the rain and no-rain samples coming from the same population.

Lovejoy and Austin (1979) attempted to further classify the cumulus rain and no-rain cases into no-rain, light rain, and heavy rain. Rainfall rates greater than 2 mm-h-1, as determined by radar, were defined as heavy rain. As expected, the mean of the heavy rain cases was shifted slightly toward higher visual and infrared values than the

mean of the light rain cases. However, the shift was so small that there was at least an 80% probability of the light rain and the heavy rain cases coming from the same population. Lovejoy and Austin (1979) concluded that "little, if any rainfall-rate information is contained in a single (visual and infrared) satellite image.

Lovejoy and Austin (1979) tested a spectral threshold technique for rain area mapping. Each satellite image of 400 x 400 km was divided into one hundred 40 x 40 km boxes. The 100 subareas were each checked with radar to determine the total number of rain areas. An equal total number of satellite subareas were classified as rain areas. The satellite subareas with the highest visual and highest (cold) infrared values were classified as rain areas, until the total number of satellite rain areas equaled the total number of radar determined rain areas. This spectral threshold technique was applied to three days accumulation of data and is shown in Tables XIII and XIV. When compared to the success of the two dimensional frequency plot method, the visible and infrared thresholds averaged 45% and 58% worse, respectively. The accuracy of the visual threshold is limited by the extent of low, thick clouds and the infrared threshold is limited by the extent of the cirrus clouds in the satellite image. Lovejoy and Austin (1979) concluded that "the errors involved in using a 'best threshold' are very large indeed."

Del Beato (1981) studied correlations between cloud top temperatures (based on NOAA-5 satellite data) and rainfall totals for 30 and 60 minute intervals over eastern Australia. The satellite data had a 60 sq km maximum resolution at subsatellite point and cloud top temperatures were area averaged for resolution of 200 sq km. The 21 data sets were first classified according to synoptic situation in a rough attempt to group the data by cloud type, droplet

39
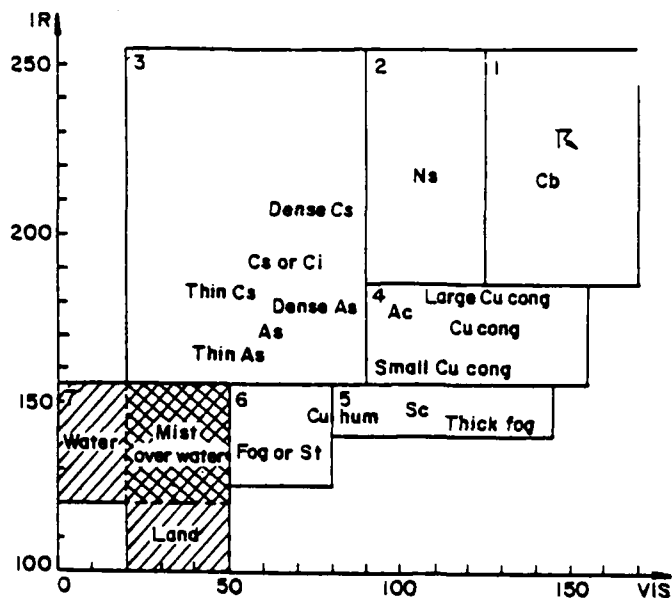
Fig. 7. Separation of Different Cloud Types in VIS
and IR from TIROS-N AVHRR-data. Sun Elevation 45
(Liljas, 1981)
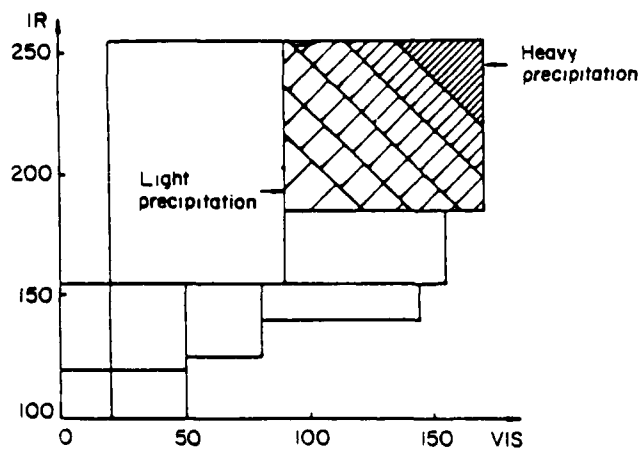
Fig. 8. Qualitative Indication of Precipitation
Intensities Derived Using VIS and IR Data from
TIROS-N AVHRR-data. (Liljas, 1981)
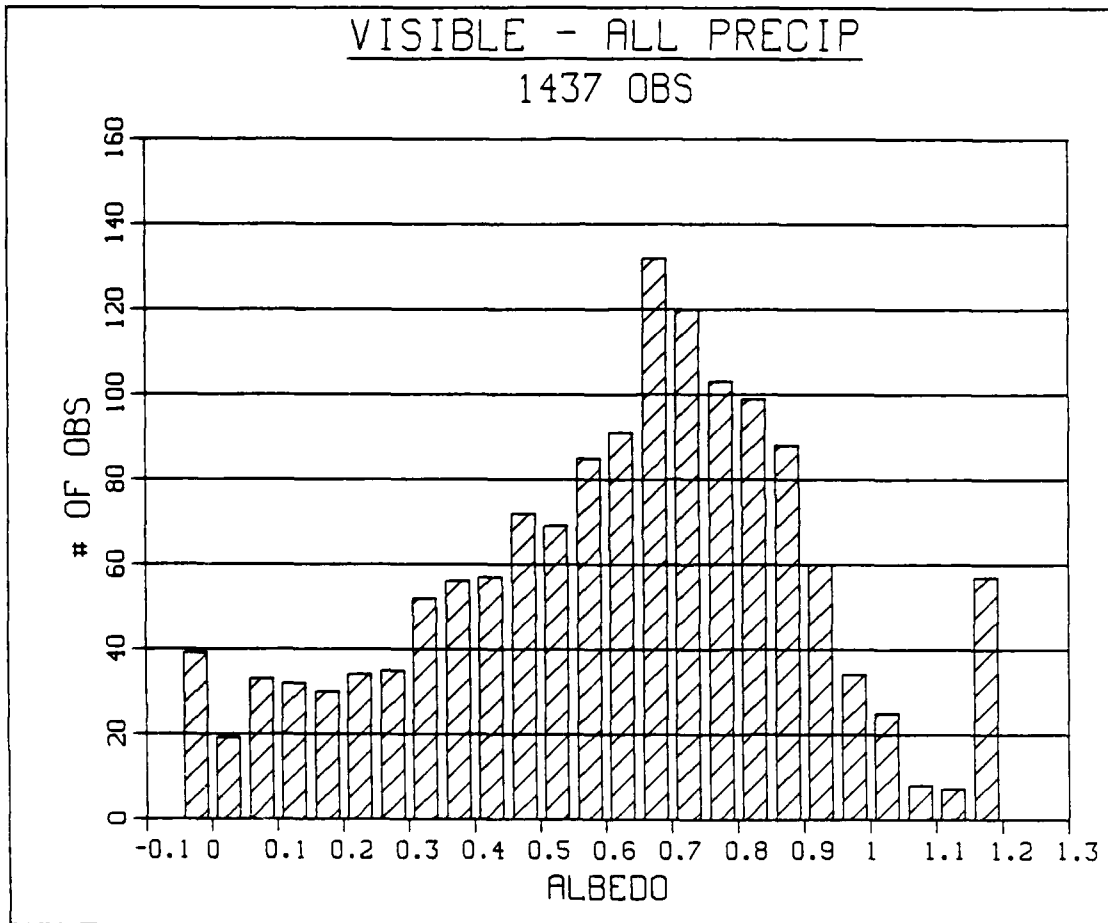
53

VISIBLE - ALL PRECIP
1437 OBS

Fig. 6. Precipitation, Visible Data Distribution

INFRARED - ALL PRECIP
1856 OBS

Fig. 5. Precipitation, Infrared Data Distribution

51

VISIBLE - ALL PRECIP (10X10)
1437 OBS
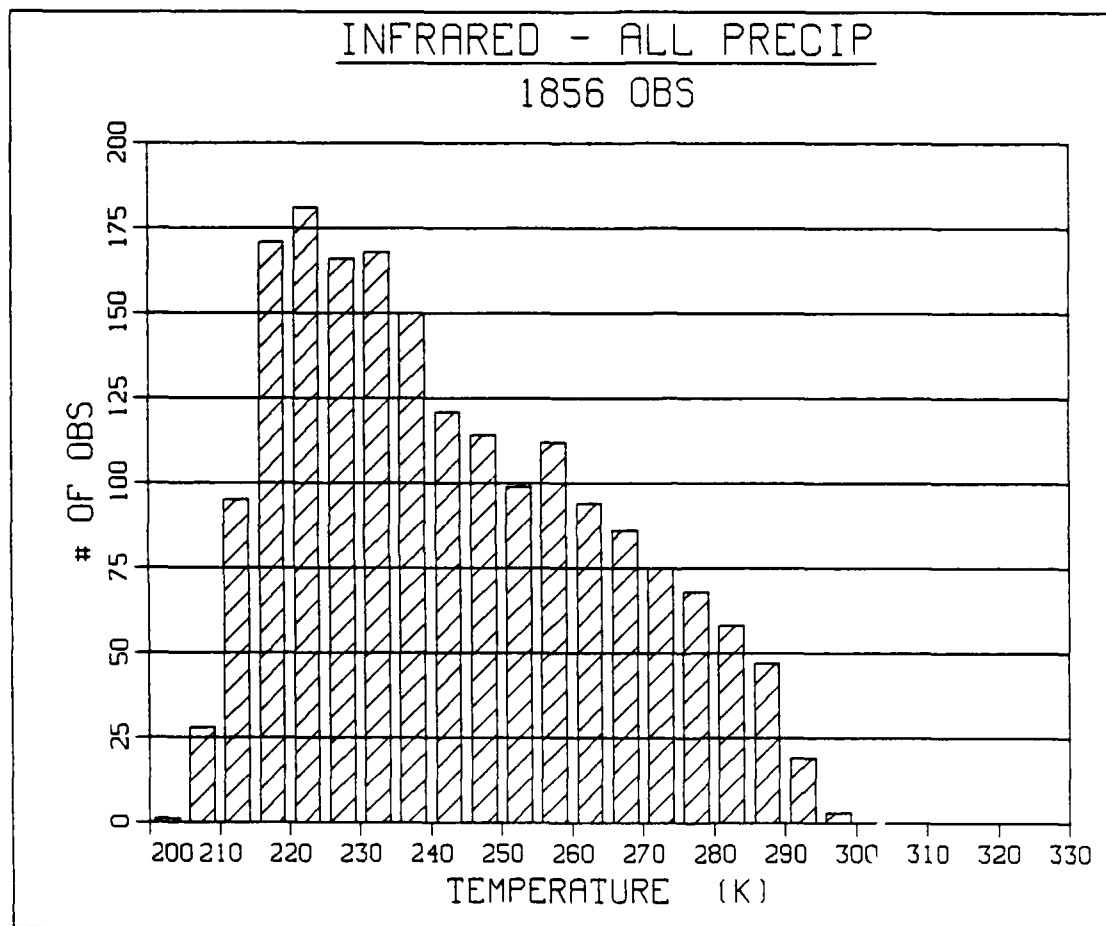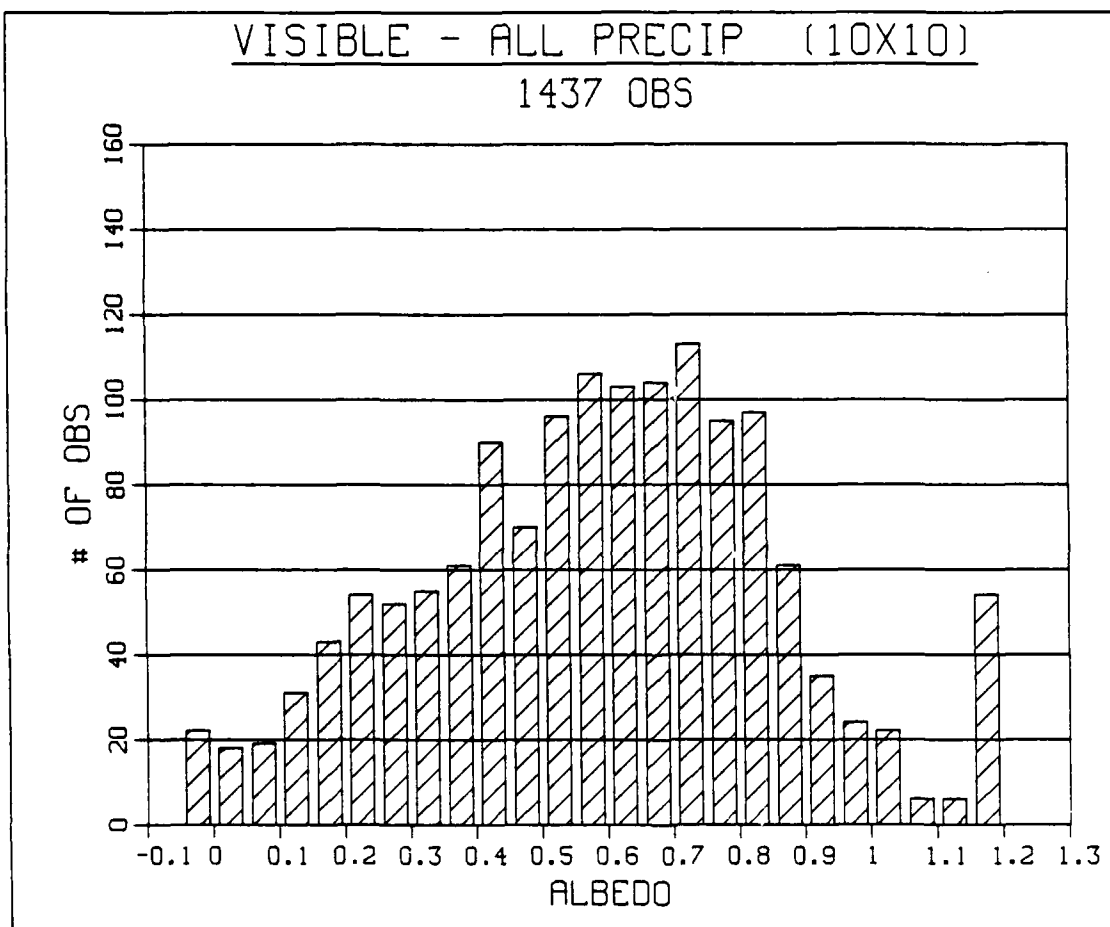
Fig. 4. Example of Non-Normal Data Distribution

VISIBLE - NO PRECIP

14,740 OBS

Fig. 3. No-Precipitation, Visible Data Distribution

49
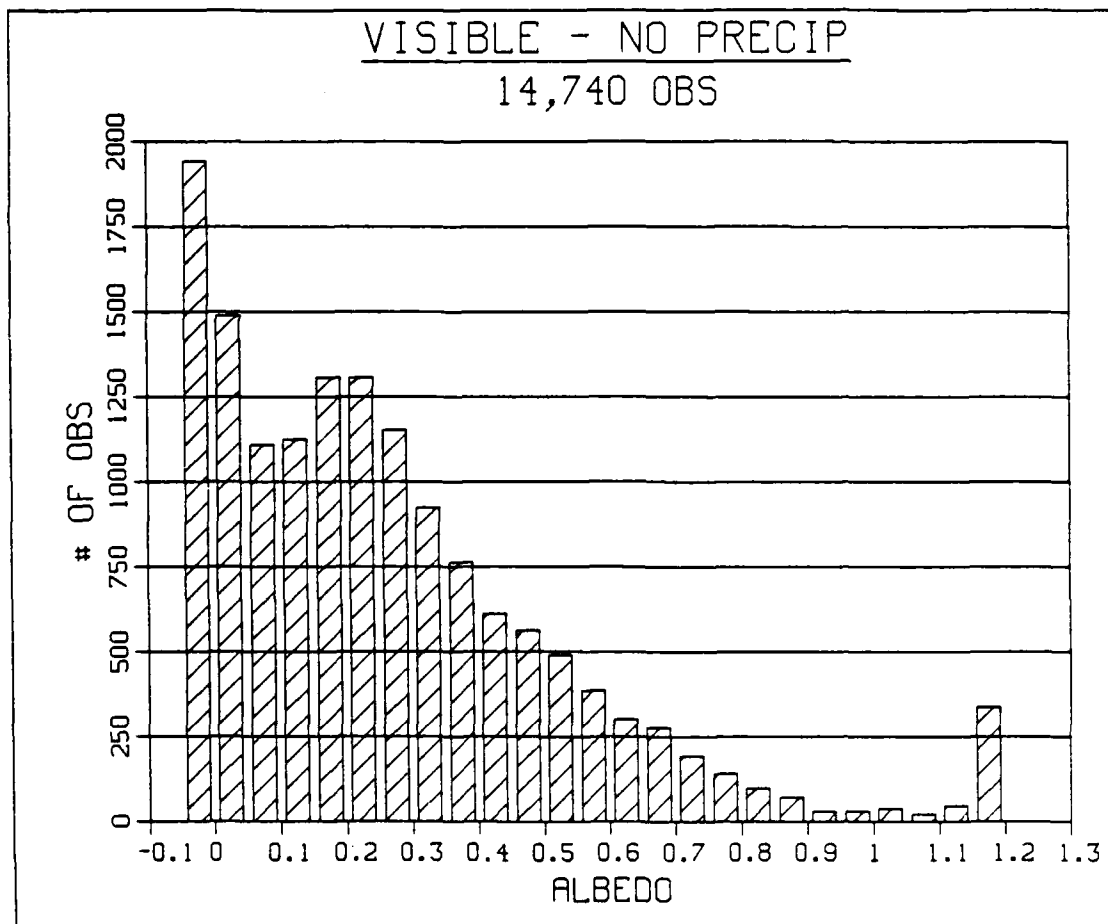
INFRARED – NO PRECIP
19,354 OBS
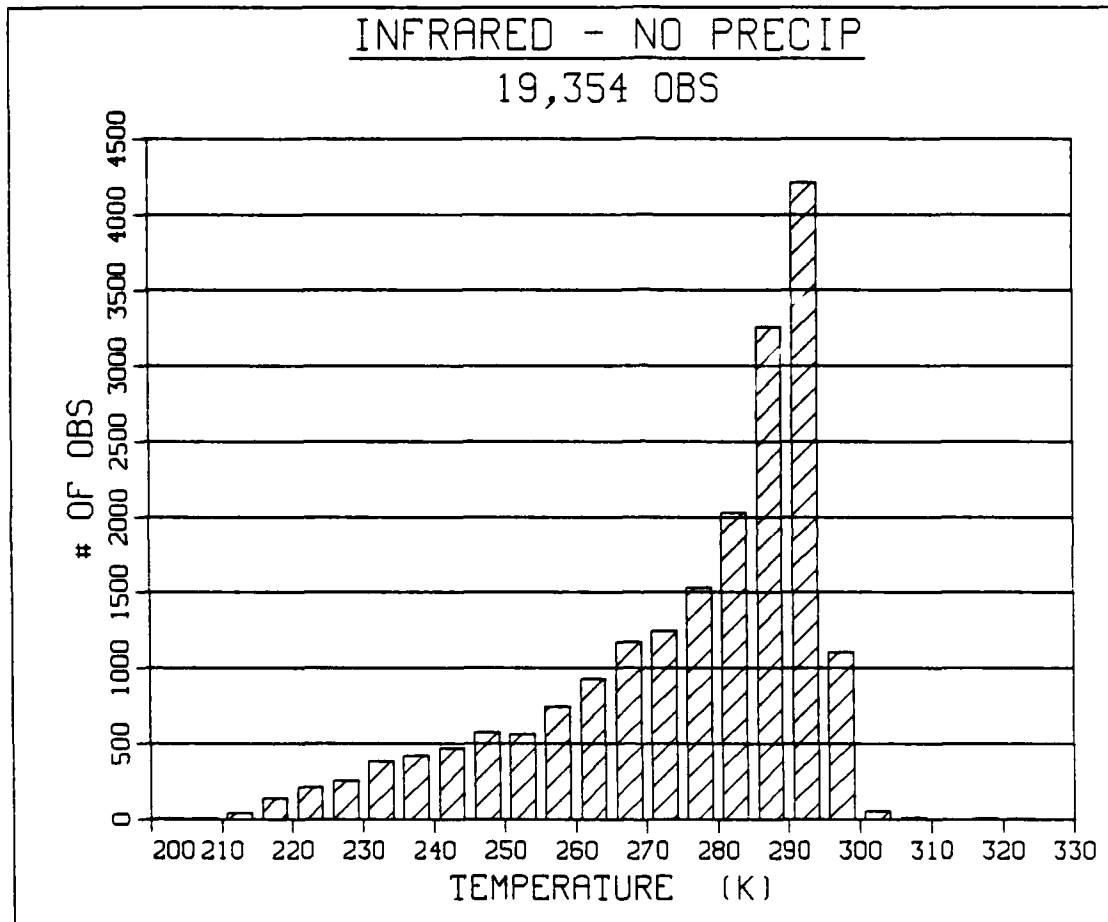
Fig. 2. No-Precipitation, Infrared Data Distribution

APPENDIX C
FIGURES
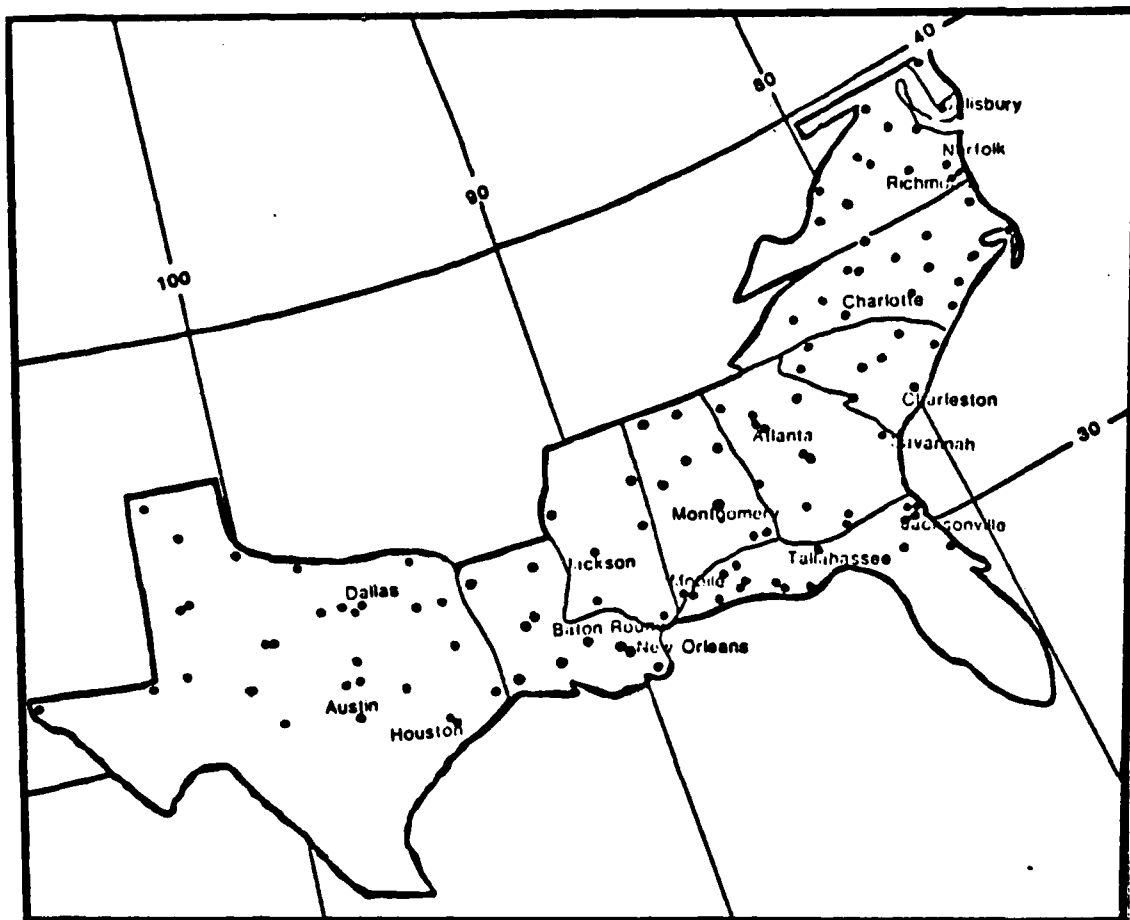
Fig. 1. Geographical Location of Service-A Station
         Station Report Data

APPENDIX B
MUENCH AND KEEGAN (1979) NORMALIZATION SCHEME

The Muench and Keegan (1979) normalization relates the normalized reflectivity (r_n) to the varying solar angle and maximum digital counts through the reflectance term $(\tilde{r})$, and the anisotropic scattering through the χ term. Table XVII defines the symbols, Table XVIII lists the geometric identity equations, and Table XIX lists the normalization equations. Fig. 11 gives an example of the normalization applied to the stated location.

the two values. The most accurate estimations were for the cumulus clouds in the warm air masses occurring in June, the cases the model was designed to handle. Wylie concluded that in order to estimate the rainfall in all geographical areas and seasons a more sophisticated model would be needed.

Negri and Adler (1981) did one case study of 15 thunderstorms in the Oklahoma, Arkansas, and Missouri area on 24 April 1975. They used radar data for ground truth and had special 5 minute GOES-E satellite passes over the area of interest. They were able to determine that precipitation began falling, as indicated by radar data, for cloud top temperatures ranging from 229 K to 260 K (-44 C to -13 C). The mean cloud top temperature value was 247 K (-26 C).

during GATE. The cloud area and its change are defined by the threshold value. The visible threshold for cloud area calculations was 60 digital counts on the ATS-3 (corresponding to an albedo of 0.45 with the sun overhead), or equivalently 172 digital counts on the Geosynchronous Meteorological Satellite (SMS 1). The infrared threshold was 160 digital counts (-26 C). The standard error between the estimated rainfall and the mean radar rainfall was 62% and 76% for the visual and infrared equations respectively.

Wylie (1979) attempted to use the tropical convective rainfall techniques of Griffith et al, (1978) and Stout et al, (1979) for estimating precipitation in Montreal, Canada. Using visual satellite data, corrected for the changing sun angle (Mosher, 1975), infrared satellite data, and 10.0 cm radar measured rainfall rates, Wylie studied six days of precipitation, three days each in June and September 1977. Wylie concluded that because of air mass differences between Montreal and the tropics, the Griffith and Stout estimation techniques did poorly in Montreal, Canada. The singlemost important limitation with these two schemes was the difficulty in measuring cumulonimbus cloud area when the "anvils were often merged into large cloud masses and the extensive stratus cloud cover often obscured the pictures." Wylie also noted that the Griffith et al, (1978) threshold of -26 C had to be changed to -16 C for the summertime Montreal, Canada area. With the warmer cloud top temperatures the cloud area were a larger, more appropriate size for tracking.

Wylie (1979) then attempted to combine sounding data input into a one-dimensional model (Simpson and Wiggert, 1969) and satellite cloud cover measurements to estimate rainfall for Montreal. With the GATE measurements for rain rates associated with satellite- derived cloud areas and the model output, rainfall rates were estimated by multiplying

(ATS-3) and the infrared threshold was 253 K (-20 C). The thresholds were based on a comparison of the clouds with a given maximum digital count and the radar echoes associated with these clouds.

The empirical cloud area-rainfall relationship was derived as a two step process. First, a relationship between the cloud area and the radar echo area, normalized for the maximum area achieved by the cloud or the cluster, was established for the visible and infrared satellite data. Second, the relationship between the echo area and the rain volume was determined and was of the form:

$$Rv = IAe \qquad\qquad (A.4)$$

where Rv is the rain volume per hour (m3 -h-1), I is rain in units of (m3 -km-2 -h-1), and Ae is the echo area (km2) defined by the 1mm -h-1 rain rate. Thus, given a time sequence of convective clouds (or cluster areas) measured from visible or infrared satellite images, a volumetric rain rate can be estimated.

Stout et al, (1979) modified the Griffith/Woodley technique (Griffith et al, 1978) to estimate volumetric rain rate directly from a cumulonimbus cloud area and area change according to the equation:

$$R = a(0)A + a(1)dA/dt \qquad\qquad (A.5)$$

where R is the volumetric rainfall of the cloud (m3 -s-1), A is the cloud area (m2), dA/dt is the change of cloud area over time (m2 -s-1), and a(0) and a(1) are constants with dimensions (m -s-1) and (m) respectively. The two constants were calculated by a least square fit of cloud area-rain rate pairs based on visible and infrared geosynchronous satellite data and 5.3 cm ship radar rain data collected

43

clouds, and second, that convective clouds can be identified
and measured in satellite images. These methods involve
manual analyses of convective cloud areas in a sequence of
visual, infrared, or both visual and infrared satellite
images. Threshold values and study condition parameters
associated with published life history studies are summa-
rized in Table XVI.

The Scofield/Oliver (Scofield, 1981) analysis follows a
decision tree procedure to estimate half-hourly rainfall for
deep convective systems within tropical air masses. Using
enhanced infrared and high resolution visual satellite
images, the technique involves first identifying the active
convective portion of the cloud, or cluster, from two
consecutive satellite images. Once the active portion is
identified, the half-hourly rainfall estimation is computed
based on such factors as cloud top temperature, cloud
growth, and departure of precipitable water from a summer-
time normal.

The Griffith/Woodley (Griffith et al, 1978) technique is
designed to estimate rainfall in the tropics, over large
space and time scales, using geosynchronous visual or
infrared satellite imagery. This time-dependent technique
was empirically derived as a relationship between cloud
area, echo area, and rain rate for two areas in south
Florida, with raingauge-radar providing the ground truth,
and was then tested in other tropical areas. This scheme
was subsequently tested further in extratropical areas
(Griffith et al, 1980), with modifications to the rainfall
amount predicted.

The determination of a cloud area-rainfall relationship
first required the specification of both a visual and an
infrared threshold to define the cloud area. The visual
brightness threshold, normalized for radiation geometry, was
80 counts for the third Application Technology Satellite

42

Wylie (1982) attempted to correlate rainfall occurrence
with radiosonde soundings, hourly Service-A observations,
and visual and infrared satellite data. His data sample was
restricted to "large-scale cloud cover" areas with wide-
spread precipitation (rain gauge reports varied less than
20%) for the Great Plains States region for the period 27
February 1981 through 4 January 1982. From 13 parameters
derived from three data sources (see Table XV) the best
linear regression equation for estimating rainfall rate was:

$$6h \text{ rain} = 1.0242 + 0.380P_w - 0.0304Q_c - 0.0047C_t \qquad (A.2)$$

where P_w is the vertically integrated precipitable water
vapor (in), Q_c is the moisture convergence (g/kg/day), and
C_t is the cloud top temperature (Kelvin). Equation A.2 has
a linear correlation coefficient of 0.60. Linear regression
equations were also determined for the three parameters
alone and for a combination of P_w and Q_c to be used when not
all three data types were available. The cloud temperature
regression equation was:

$$6h \text{ rain (in)} = 2.10 - 0.008C_t \qquad (A.3)$$

The correlation coefficient was -0.35. Wylie (1982) stated
that the synoptic scale data base measurements were best
suited for estimating broad changes in rainfall rates asso-
ciated with air masses and not suited for estimating rain-
fall rates associated with small scale dynamic processes.

B. LIFE HISTORY

The life history methods are empirically derived precip-
itation estimation schemes based upon two assumptions,
first, that significant rainfall comes from convective

41

spectra, and air mass trajectory. The initial results suggested that the cloud top temperature determined an upper limit on rainfall amount, with the maximum increasing as the cloud top temperature decreases. A linear correlation analysis to determine a quantitative relationship between rainfall amount and cloud top temperature gave indefinite results.

Further study of surface and radiosonde observations indicated that classification by proportion of cumuliform cloud reports to all cloud reports and subcloud layer humidity might be more appropriate (Del Beato, 1981). This classification resulted in a correlation coefficient of 0.90, excluding cases with cumuliform portions less than 50% and dew point depressions of greater than 6 C. Finally a composite frequency distribution was calculated based on three cases, all southwesterly stream situations described as "post-frontal cellular convection cases in cyclonically curved flow." The fitted equation was:

$$f = 0.057 - 0.004CTT - 0.054R \tag{A.1}$$

where f is the rainfall frequency, R is the 30 minute rain total (mm), and CTT is the cloud top temperature in degrees Celsius. The equation was fitted to 41 independent f values. This equation is associated with a correlation of 0.79 at the 99% confidence level. Equation A.1 indicates no rain from clouds warmer than +13 C and a maximum 30 minute rainfall of 2.5 mm for a cloud top temperature of -20 C.

In summary, Del Beato (1981) found that cloud top temperatures and 30 and 60 minute rainfall totals indicated statistically significant relationships for cloud systems with a high portion of cumulus clouds and high subcloud humidity. Additionally, as cloud top temperatures decrease to at least -35 C, rainfall totals increase.

Fig. 9. Frequency Plot of Rain Data Distribution for GATE day 248, 1300 GMT (Lovejoy and Austin, 1979)

Fig. 10. Frequency Plot of No-Rain Data Distribution for GATE day 248, 1300 GMT (Lovejoy and Austin, 1979)
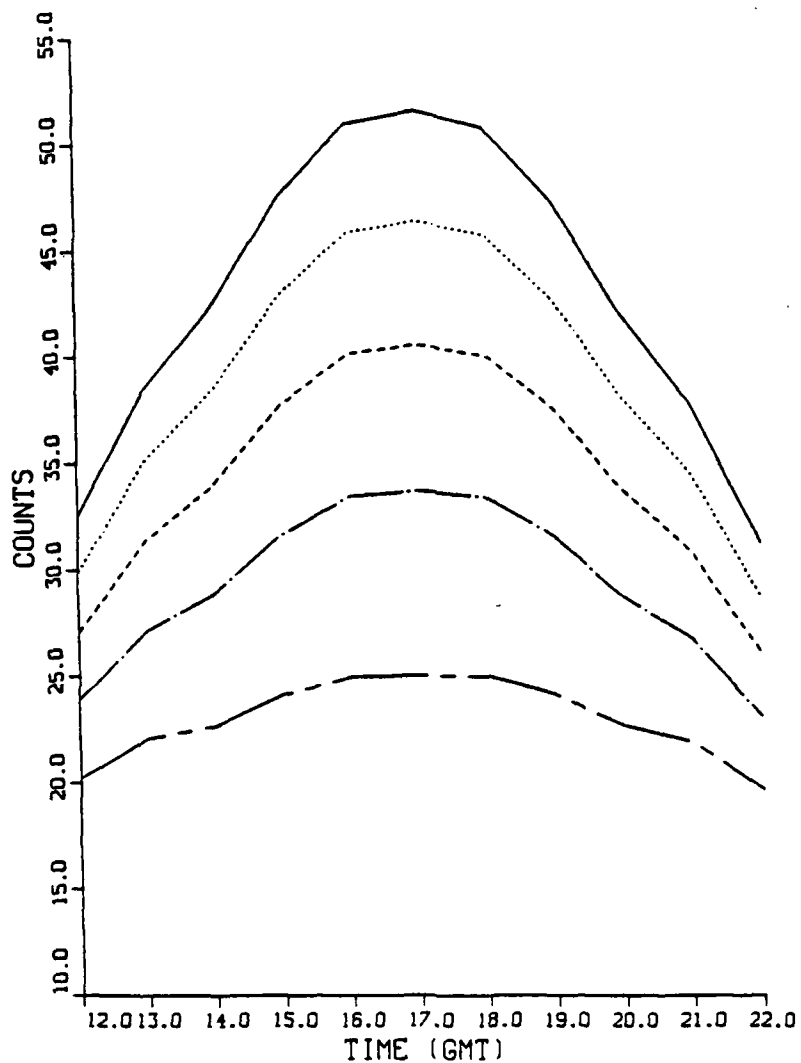
Fig. 11. Normalized Cloud Reflectivity as a Function of
Video Count and Time of Day for 16 April 1977
at 42 N and 74 W with Calibration Count Equal
to 60   (Muench and Keegan, 1979)

55

APPENDIX D
TABLES

Table I.   Information Available for Each Observation

1.   Station ID
2.   Latitude
3.   Longitude
4.   Altimeter
5.   Temperature
6.   Dew Point
7.   Wind Direction
8.   Wind Speed
9.   Sea Level Pressure
10. Cloud Group
11. Visibility
12. Precipitation Amount
13. Wind Gusts
14. Current Weather
15. Maximum Temperature
16. Minimum Temperature
17. Snow
18. Observation Date/Time
19. Visible/Infrared Satellite Data

Table II.   Comparison of Means and Standard Deviations
             of Each Matrix Size for Each Category

No Precip IR	10 x 10	8 x 8	6 x 6	4 x 4
Mean	275.82	275.88	275.74	275.71
St Dev	18.37	18.69	19.03	19.37

All Precip IR				
Mean	244.61	244.00	243.47	242.99
St Dev	21.05	21.26	21.46	21.72

No Precip VIS				
Mean	26.91	27.02	27.15	27.29
St Dev	24.96	25.29	25.72	26.32

All Precip IR				
Mean	58.69	59.63	60.57	61.32
St Dev	27.15	27.40	27.90	28.53

57

Table III.   No-Precipitation, Infrared Analysis

Mean: 275.71   St Dev: 19.37

COLD TAIL: 1461 Obs   (< 240.0 K)

	# Obs	High	Middle	Low
Overcast	0.50	0.35	0.10	0.05
Broken	0.50	0.41	0.07	0.03
Total	1.00	0.76	0.16	0.08

Table IV.   No-Precipitation, Visible Analysis

Mean: 27.29   St Dev: 26.32

BRIGHT TAIL: 999 Obs   (> 0.70)

	# Obs	High	Middle	Low
Overcast	0.49	0.18	0.14	0.17
Broken	0.51	0.41	0.07	0.03
Total	1.00	0.59	0.22	0.20

Table V.   Precipitation, Infrared Analysis

Mean: 242.99   St Dev: 21.72

	Cold End	Middle Region	Warm Tail
TRW	0.15	0.05	0.06
TRW-	0.42	0.21	0.18
RW	0.02	0.04	0.02
RW-	0.20	0.37	0.50
R	0.02	0.01	0.01
R-	0.14	0.29	0.21
TR	0.00	0.01	0.00
TR-	0.05	0.03	0.02
# Obs	959	626	257

Table VI.   Precipitation, Visible Analysis

Mean: 61.32   St Dev: 28.53

	Bright End	Middle Region	Dim Tail
TRW	0.18	0.11	0.08
TRW-	0.29	0.29	0.28
RW	0.06	0.03	0.02
RW-	0.19	0.30	0.43
R	0.03	0.02	0.01
R-	0.21	0.22	0.15
TR	0.01	0.01	0.00
TR-	0.03	0.02	0.03
# Obs	163	916	327

Table VII.   Comparison of Means and Standard Deviations for
Precipitation with Broken/Overcast Ceilings
with Paul (1983).   (Paul's values in
parenthesis)

Precipitation - Infrared

	10 x 10		4 x 4	
Mean	244.6 K	(252.8 K)	243.0 K	(250.6 K)
St Dev	21.1 K	(20.5 K)	21.7 K	(21.5 K)

Precipitation - Visible

	10 x 10		4 x 4	
Mean	0.587	(0.580)	0.613	(0.617)
St Dev	0.272	(0.210)	0.285	(0.225)

Table VIII.   Comparison of Means and Standard Deviations for
No-Precipitation with Broken/Overcast Ceilings
with Paul (1983).   (Paul's values in
parenthesis)

No-Precipitation - Infrared

	10 x 10		4 x 4	
Mean	275.8 K	(279.8 K)	275.7 K	(279.7 K)
St Dev	18.4 K	(16.6 K)	19.4 K	(17.8 K)

No-Precipitation - Visible

	10 x 10		4 x 4	
Mean	0.269	(0.271)	0.273	(0.277)
St Dev	0.250	(0.189)	0.263	(0.207)

Table IX.   Verification of SPADS Infrared Thresholds

Satellite Estimate: Observations:	Yes	No	Total Obs
Yes	1195 (0.64)	661 (0.36)	1856
No	2503 (0.13)	16,851 (0.87)	19,354
Total Obs	3698	17,512	21,210

Table X.   Verification of SPADS Visible Thresholds

Satellite Estimate: Observations:	Yes	No	Total Obs
Yes	909 (0.63)	528 (0.37)	1437
No	1962 (0.13)	12,778 (0.87)	14,740
Total Obs	2871	13,306	16,177

Table XI.   Verification of SPADS Visible and Infrared
              Thresholds Combined

Satellite Estimate Observations:	Yes	No	Total Obs
Yes	843 (0.82)	180 (0.18)	1023
No	825 (0.07)	10,319 (0.93)	11,144
Total Obs	1668	10,499	12,167

Table XII.   Threshold Values Describing Precipitation
             Intensity Levels as Applied in Fig. 8
             (Liljas, 1981a)

The Sum of Digital Levels

Ch1 + Ch 4	291 - 310	Light Rain
	311 - 330	
	331 - 350	
	351 - 370	
	371 - 390	
	399 +	Very Strong Rain

Table XIII.   Statistical Comparison of Rain Area Mapping
              Techniques   (Lovejoy and Austin, 1979)

Day	Opt. 2-D Boundary $(R_s/R) \times 100$[*]	IR Optimum Threshold IR(K)	$(R_s/R) \times 100$	Visible Optimum Threshold (Scale: 0-1)	$(R_s/R) \times 100$	Area Rain Coverage (%)	Total No. of Points
GATE							
242, 243, 246 247, 248, 251 252, 261	65	<232	53	>0.68	64	15.8	47706
Montreal							
152	56	<232	20	>0.88	31	9.7	40361
180	56	<247	55	>0.80	48	24.0	33738
153	53	<254	52	>0.88	49	15.9	22558

[*]Referred to in text as "percentage of correct satellite rain."

Table XIV.   Statistical Comparison of the Accuracy of Rain
             Areas   (Lovejoy and Austin, 1979)

Technique	Region	Number of Images or Sequences	Bias	Error Factor	E_{RMS}
2-D Pattern Matching	Montreal	17	1.13	1.26	0.22
2-D Pattern Matching	Montreal	3	1.08	1.19	0.18
Optimum IR Threshold	Montreal	3	1.38	1.74	0.71
Optimum Visible Threshold	Montreal	3	1.54	1.59	0.58
2-D Pattern Matching	GATE	8	1.21	1.41	0.25

Table XV.   General Coefficients for the Determination of
             Precipitation Based on the Three Data Types
             (Wylie, 1982)

MEASURED PARAMETER	CORRELATION WITH 6 HOUR PRECIP. REPORT	NUMBER OF CASES	F
Vertically integrated precipitable water vapor	0.48	196	58*
Cloud top brightness	-0.44	184	44*
Cloud top height	-0.40	190	36*
Moisture convergence	0.38	184	31*
Cloud top temperature	-0.35	199	27*
Bubble model predicted cond.	0.27	115	9
500 mb vorticity advection	-0.21	173	8*
Parcel lifted index	-0.20	200	8*
700 mb temperature advection	0.20	173	7*
Sfc temperature advection	0.19	156	6
850 mb temperature advection	0.17	189	6
Wind convergence (sfc)	0.09	167	1
Vertical wind shear	0.03	156	0

* Significant correlation at the 99% level.

63

Table XVI.   Summary of Life History Threshold Values

STUDY	LOCATION	CASES	TIME OF YEAR	THRESHOLD INFRARED	VALUE VISUAL
Griffith, et al., (1978)	Florida, Venezuela, Honduras, and hurricanes impacting East Coast United States	34 days	summers 1969-1976	-20°C	80 counts[*]
Stout, et al., (1979)	tropical North Atlantic	57 obser-vations	September 1974	-26°C	0.45 albedo (sun over-head)
Wylie (1979)	Montreal	6 days	June 1977 September 1977	-16°C	-
Negri and Adler (1981)	Oklahoma, Arkansas, Missouri	1 day (15 thunder-storms)	April 24, 1975	-27°C	-

[*] ATS-3 satellite

Table XVII. List of Symbols

Symbol	Description	Units
C	GOES video count number (0-63)	dimensionless
C_o	GOES video count number for perfect diffuse reflector and overhead sun	dimensionless
G	Greenwich meridian time	hours-minutes-seconds
R	Distance of earth to sun	km
R_o	Mean distance of earth to sun	km
d	Julian date	dimensionless
h	Hour angle	radians
r	Cloud reflectivity	dimensionless
γ	Arc-length observer to subsatellite point	radians
δ	Declination of the sun	radians
ζ	Zenith angle of the sun	radians
Λ	Longitude	radians
Λ_s	Longitude of subsatellite point	radians
χ	Anisotropic scattering coefficient	dimensionless
ϕ	Latitude	radians
ϕ_1	Azimuth of the sun	radians
ϕ_2	Azimuth of the satellite	radians

65

Table XVIII. Basic Geometric Satellite-Earth Relationships *

Declination:

$$\delta = 0.408 \sin [(d-81) * 2\pi/365]$$

Solar distance ratio:

$$R/R_o \stackrel{=}{=} 1 - 0.167 \cos [(d-14) * 2\pi/365]$$

Hour angle:

$$h \stackrel{=}{=} \Lambda + \pi - G(hours) \times \pi/12$$

Arc-length:

$$\cos\gamma = \cos(\Lambda_s - \Lambda) \cos\phi$$

Satellite azimuth:

$$\sin (\phi_2 - \pi) = \sin (\Lambda_s - \Lambda)/\sin\gamma$$

Solar azimuth angle:

$$\cos\zeta = \sin\phi \sin\delta + \cos\phi \cos\delta \cos h$$

Solar azimuth:

$$\sin\phi_1 = \cos\delta \sin h/\sin\zeta$$

* Angles in radians

Table XIX.   Muench and Keegan (1979) Normalization
              Equations *

$$\tilde{r} = (\frac{C}{C_o})^2 * \sec\zeta$$

$$\Delta\phi = |\phi_2 - \phi_1|$$

$$C_1 = \cos^2 ((\zeta - 50) * 1.8)$$

$$C_2 = 0.7 \cos ((\zeta - 22.5) * 4) * (1 - \cos\zeta)$$

$$C_3 = \cos^8 ((\Delta\phi - 70) * 1.3)$$

$$\chi \stackrel{=}{=} 1.0 + 0.05 * (1 + \cos(2*\zeta)) + 0.20 * (C_1 + C_2) * C_3$$

$$\tilde{r}_n = [1.09 - 2*(1.09 - \tilde{r} * \chi *(R/R_o)^2)/(1 + \cos^{1/2} \zeta)]$$

* Angles in degrees

66

LIST OF REFERENCES

Del Beato, R., 1981: The relationship between extratropical rainfall and satellite cloud-top temperatures. *Aust. Met. Mag.*, *29*, 125-131.

Griffith, C. G., J. A. Augustine, and W. L. Woodley, 1980: Satellite estimation in the U. S. high plains. *J. Appl. Meteor.*, *20*, 53-66.

Griffith, C. G., W. L. Woodley, P. G. Grube, D. W. Martin, J. Stout and D. N. Sikdar, 1978: Rain estimation from geosynchronous satellite imager--visible and infrared studies. *Mon. Wea. Rev.*, *106*, 1153-1171.

Liljas, E., 1981a: Analysis of cloud and precipitation through an automated classification of AVHRR data. RMK 32, SMHI (in Swedish), 33 pp.

Liljas, E., 1981b: Automated techniques for satellite imager analysis. *Proc. IAMAPS Symposium*, Hamburg, 25-28 Aug. 1981, 331-339.

Lovejoy, S. and G. L. Austin, 1979: The delineation of rain areas from visible and IR satellite data for Gate and mid-latitudes. *Atmos-Ocean*, *17*, 77-92.

Muench, H. S. and T. J. Keegan, 1979: Development of techniques to specify cloudiness and rainfall rate using GOES imagery data. AFGL-TR-79-0255, AD A084, 46 pp.

Mosher, F., 1975, Appendix to: D. W. Martin, J. Stout, and D. N. Sikdar, 1975: GATE area rain estimation from satellite images. Report, NOAA Grant 04-5-158-47, Space Science and Engineering Center, University of Wisconsin-Madison.

Negri, A. J. and R. F. Adler, 1981: Relation of satellite-based thunderstorm intensity to radar-estimated rainfall. *J. Appl. Meteor.*, *20*, 289-300.

Paul, L. S., 1983: *A study of precipitation occurrence using visual and infrared satellite data.* M.S. thesis, Naval Postgraduate School.

Scofield, R. A., 1981: Visible and infrared techniques for flash flood, hydrological, and agricultural applications. In, D. Atlas and O. W. Theile (editors), _Precipitation Measurements from Space, Workshop Report, October 1981_, NASA, Goddard Space Center, Greenbelt, Md., D145-D152.

Simpson, J. and V. Wiggert, 1969: Models of precipitating cumulus towers. _Mon. Wea. Rev._, _89_, 471-489.

Stout, J., D. W. Martin and D. N. Sikdar, 1979: Estimating GATE rainfall from geostationary satellite images. _Mon. Wea. Rev._, _107_, 585-598.

U. S. Department of Commerce, 1980: Surface Observations. Federal Meteorological Handbook (FMH-1B) (also NAVAIR 50-1D-1).

U. S. Department of Commerce, 1983, National Oceanic and Atmospheric Administration, National Environmental Satellite Data and Information Service, _GOES User's Guide_, by J. Dane Clark, p. 3-1.

Wash, C. H., L. Chou and L. Spray, 1984: Geostationary Satellite Cloud and Precipitation Analysis Using an Interactive Computer System. _Proc. Nowcasting-II Symposium_, Norrkoping, Sweden, 3-7 Sep. 1984, 123-127.

Wylie, D. P., 1979: An application of a geostationary satellite rain estimation technique to an extratropical area. _J. Appl. Meteor._, _18_, 1640-1648.

Wylie, D. P., 1982: Some statistics for combining radiosonde soundings with satellite images for estimating rainfall. Report, NOAA Contract NA-80-SAC-00721, Space Science and Engineering Center, University of Wisconsin-Madison, 23 pp.

INITIAL DISTRIBUTION LIST

		No. Copies
1.	Defense Technical Information Center Cameron Station Alexandria, Virginia 22314	2
2.	Library, Code 0142 Naval Postgraduate School Monterey, California 93943	2
3.	Ccmmander Naval Oceanography Command NSTI Station, Mississippi 39529	1
4.	Ccmmanding Officer Fleet Numerical Oceanography Center Monterey, California 93940	1
5.	Officer-in-Charge Naval Environmental Prediction Research Facility Monterey, California 93940	1
6.	Dr. R. J. Renard, Code 63Rd Naval Postgraduate School Monterey, Califcrnia 93943	1
7.	Dr. C. N. K. Mooers, Code 68Mr Naval Postgraduate School Monterey, California 93943	1
8.	Department of Meteorology Library, Code 63 Naval Postgraduate School Monterey, California 93943	1
9.	Program Manager AFII/CIRF Wright-Patterson AFB, Ohio 45433	1
10.	Air Weather Service Technical Library Scott AFB, Illinois 62225	1
11.	Captain David W. Rust 2nd Weather Wing APO New York 09021	4
12.	Director of Research and Administration, Code 012 Naval Postgraduate School Monterey, California 93943	1
13.	Dr. C. H. Wash, Code 63Wx Naval Postgraduate School Monterey, California 93943	12
14.	Dr. J. S. Boyle, Code 63Xj Naval Postgraduate School Monterey, California 93943	1

END

FILMED

6-85

DTIC